AGU PUBLICATIONS

JGR

Journal of Geophysical Research: Space Physics

RESEARCH ARTICLE

10.1002/2013JA019222

Key Points:
- Particle-based model for plume/ionosphere interactions
- Charge exchange reactions modeled using detailed DCS/TCS data
- *B* field has a strong influence on the development of plumes

Correspondence to:
K. A. Stephani,
kstephan@umich.edu

Citation:
Stephani, K. A., and I. D. Boyd (2014), Detailed modeling and analysis of spacecraft plume/ionosphere interactions in low Earth orbit, *J. Geophys. Res. Space Physics*, *119*, 2101–2116, doi:10.1002/2013JA019222.

Received 12 JUL 2013
Accepted 21 JAN 2014
Accepted article online 27 JAN 2014
Published online 1 MAR 2014

Detailed modeling and analysis of spacecraft plume/ionosphere interactions in low Earth orbit

K. A. Stephani[1] and I. D. Boyd[1]

[1]Department of Aerospace Engineering, University of Michigan, Ann Arbor, Michigan, USA

Abstract Detailed direct simulation Monte Carlo/particle-in-cell simulations involving the interaction of spacecraft thruster plumes with the rarefied ambient ionosphere are presented for steady thruster firings in low Earth orbit (LEO). A nominal mass flow rate is used to prescribe the rocket exit conditions of a neutral propellant species for use in the simulations. The charge exchange interactions of the steady plume with the rarefied ionosphere are modeled using a direct simulation Monte Carlo/particle-in-cell methodology, allowing for a detailed assessment of nonequilibrium collisional and plasma-related phenomena relevant for these conditions. Results are presented for both ram- and wake-flow configurations, in which the thrusters are firing into (ram) or in the direction of (wake) the free stream ionosphere flow in LEO. The influence of the Earth's magnetic field on the development of the ion plume is also examined for three different field strengths: two limiting cases in which $B \rightarrow 0$ and $B \rightarrow \infty$, and the LEO case in which $B = 0.5$ Gs. The magnetic field is found to have a substantial impact on the resulting neutral and ion plumes, and the gyroscopic motion of the magnetized ions results in a broadening of the ion energy distribution functions. The magnetic field model also incorporates a cross-field diffusion mechanism which is shown to increase the current density sampled far from the thruster.

1. Introduction

Spacecraft thruster firings occur often in low Earth orbit as a means of altering the trajectory of a space vehicle. A fundamental understanding of plume dynamics in this rarefied plasma environment is imperative for developing both predictive and mitigatory capabilities to avoid plume impingement on critical spacecraft surfaces. Chemical interactions between postcombustion neutral species generated by spacecraft thrusters and ambient ions in the upper atmosphere play an important role in determining the dynamic behavior of these plumes. In particular, the high-density neutral plume emitted during a thruster burn is subject to charge exchange reactions with the ambient ions. This interaction can alter the local ionospheric properties and lead to excitation of plasma waves. Studies of such interactions, both experimental and computational, have been centralized around low Earth orbit (LEO) transportation spacecraft, including Space Shuttle Soyuz, Progress, and the Mir space station [e.g., *Burke et al.*, 1995; *McMahon et al.*, 1983; *Karabadzhak et al.*, 1997; *Drakes and Swann*, 1999; *Kaplan and Bernhardt*, 2010; *Bernhardt et al.*, 2012].

In particular, the study by *Burke et al.* [1995] examined the energy distribution of positive, single-charge ions detected by the Shuttle Potential and Return Electron Experiment (SPREE) during a thruster burn of the Tethered Satellite System (TSS 1) mission. Data collected by this sensor included information regarding both energy and angular distributions of ions impacting the sensor, over ion energies ranging from 10 to 100 eV. This study also compared SPREE data with results from a two-dimensional collisionless molecular model. The model tracked trajectories of neutrals and pick up ions (plume-related ions formed through charge transfer of plume neutrals with ambient ions) during a thruster burn event and provided information regarding the distribution of ions that eventually impact the SPREE sensor. This allowed for a comparison between the measured and predicted ion energy distributions. It was also found that significant scattering occurs near the thruster exit as well as after charge exchange between the neutral gas and ambient oxygen ions.

The present study aims to examine the interaction between spacecraft thruster plumes and the ambient ionosphere in low Earth orbit conditions. While previous work has examined near-field plume/ionosphere interactions, this study will focus on nonequilibrium collisional and plasma-related phenomena over extended distances of many kilometers. The rarefied nature of the ionosphere, as well as the surrounding plasma, requires the use of a combined direct simulation Monte Carlo/particle-in-cell (DSMC/PIC)

Table 1. Permitted Interactions Between Plume/Ambient Chemical Species

	Pr	Pr^+	O	O^+
Pr	MEX	MEX/CEX	MEX	MEX/CEX
Pr^+	–	–	MEX	–
O	–	–	MEX	MEX
O^+	–	–	–	–

methodology, which is detailed next. It is assumed that the neutral rocket plume is comprised of a single propellant species. Results are presented for a steady spacecraft thruster burn, with two rocket plume configurations examined. The effects from the geomagnetic field on the development and propagation of the ion plume is also investigated. Specifically, three magnetic field strengths are examined: two limiting cases in which the ion plume develops in the absence of a magnetic field as well as in an infinitely strong magnetic field and a third intermediate case in which the field strength is equivalent to that at LEO. Finally, conclusions drawn from this study are presented, and direction for future work is discussed.

2. Modeling of Plume/Ionosphere Interactions

2.1. DSMC/PIC Framework

The charge exchange collisions between ambient ions and rocket plume propellant occur under very low density conditions. The most appropriate numerical method for simulation of these phenomena is the direct simulation Monte Carlo (DSMC) method [*Bird*, 1994]. The plasma formed in this process is subject to self-consistent electrostatic fields, which are most appropriately modeled using the particle-in-cell (PIC) method [*Birdsall and Langdon*, 2004]. The combination of rarefied collisional and plasma phenomena relevant to the physical system of interest is therefore analyzed using Monaco PIC (MPIC) [*Cai*, 2005], which uses the DSMC solver (referred to as Monaco) solver (referred to as Monaco) and PIC methods simultaneously to model the flow field. The combined DSMC/PIC method in this work uses an unstructured computational mesh which facilitates calculation of the DSMC collisions, as well as both the self-consistent electric field and external geomagnetic field forces imposed on charged particles in the system. The MPIC solver uses a combined kinetic/fluid approach to model the plasma environment, and it is assumed that the plasma is quasi-neutral. Heavy (neutral and ion) species are modeled as DSMC macroparticles, while the electrons are represented as an equilibrium electron fluid.

Heavy particle collisions within the computational cells are computed first using a species-specific implementation of the No Time Counter (NTC) method [*Bird*, 1994], and the collision cross sections employed in this work are outlined in the next section. A species-specific conservative weighting scheme [*Boyd*, 1996] is used for improved statistics of species characterized by low number densities, as the number densities of chemical species in these simulations span many orders of magnitude.

After the binary collisions are processed, but before particles are moved, the particle-in-cell approach is used to determine the acceleration on the charged particles by the self-consistent electric field. The electron

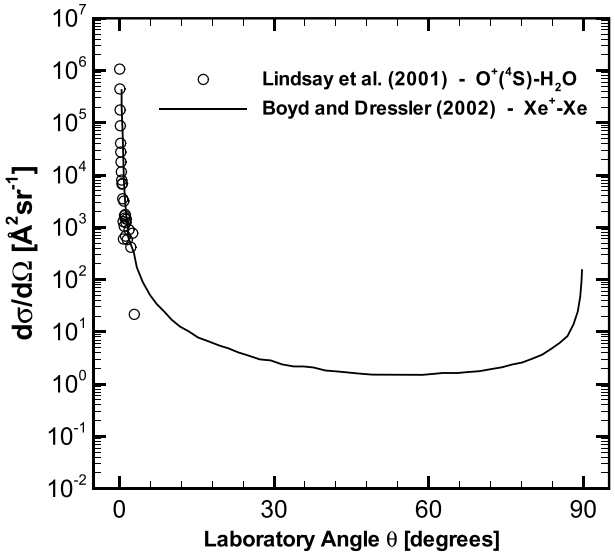

Figure 1. Differential cross sections (DCS) used for modeling charge exchange collision dynamics of $O^+ - Pr$ system.

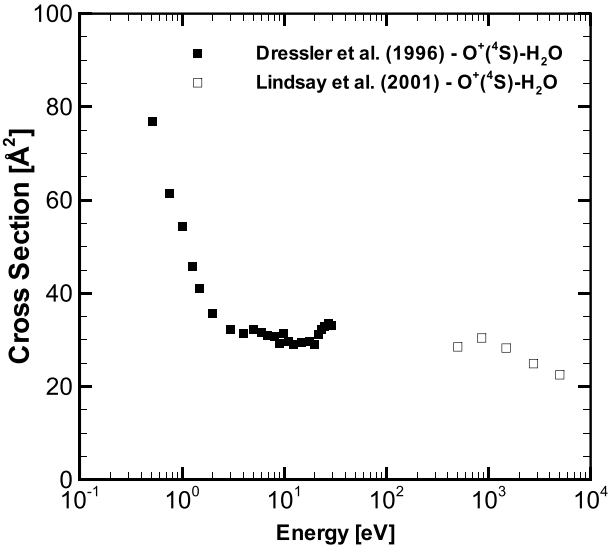

Figure 2. Total cross sections (TCS) used for modeling charge exchange collision dynamics of $O^+ - Pr$ system.

charge density is first interpolated onto each computational node, assuming that the electrons track the ion macroparticles in the computational cells. The local potential is then determined through the Boltzmann relation, which approximates the plasma potential ϕ according to

$$\phi = \phi_r + T_e \log\left(\frac{n_e}{n_r}\right), \tag{1}$$

where ϕ_r and n_r are the reference electron potential and reference electron number density, respectively, T_e is the electron temperature (eV), and n_e is the electron number density which follows from the ion number density under the assumption of quasi-neutrality. It is important to note that the use of the Boltzmann relation invokes several assumptions, namely that the electron flow is isothermal, ideal, and the influence of a magnetic field is neglected in the electron momentum equation. The electric field is then determined as

$$E = -\nabla\phi, \tag{2}$$

and the resulting acceleration is imposed as a velocity increment on the ions at each time step. In addition to the electric field acceleration, the geomagnetic field acceleration is also imposed on the ions prior to advancing the simulation time step. The magnetic field model for the heavy ion particles is detailed later in section 2.3.

2.2. Charge Exchange/Momentum Exchange Collision Dynamics

The chemical system under consideration is comprised of four chemical species: spacecraft neutrals/ions and ambient (ionosphere) neutrals/ions. The spacecraft thrusters eject a high-density plume of neutral particles, comprised mostly of water vapor, which expands into the surrounding ambient flow. It is assumed that the spacecraft neutral plume constituents are modeled as a single propellant species with a corresponding ion, referred to as Pr and Pr^+. The molecular weight of the Pr species is equivalent to the molecular weight of the neutral plume mixture, and the collisional properties of Pr and Pr^+ follow those of water vapor. The ambient ionosphere model used in this study is comprised of the primary neutral and ion species found at LEO, O, and Pr^+. Interaction of Pr with the ambient Pr^+ leads to the formation of Pr^+ through a charge exchange (CEX) reaction.

Table 2. VHS Parameters for $Pr - O$, $O - O$, and $Pr - Pr$

	d_{ref}	T_{ref}	ω
Pr	4.0 Å	273 K	0.75
O	3.0 Å	273 K	0.75

The O^+ ions are allowed to participate in both momentum exchange (MEX) and CEX interactions, but the postcollision properties of O^+ are not updated. As will be discussed later in this section, this effectively models the O^+ as being trapped indefinitely on the geomagnetic field lines. The neutral O atoms are allowed to participate in MEX interactions only, but the postcollision properties are updated. This serves to preserve the ratio of ambient O^+ ions and O neutrals throughout the computational domain. Both Pr and

Pr^+ participate in MEX/CEX interactions. A summary of the permitted interactions for this chemical system are provided in Table 1. The rotational and vibrational internal structure of plume constituents (Pr, Pr^+) is neglected in this work.

Heavy particle interactions are treated according to standard DSMC collision dynamics, with the possibility of a charge transfer for neutral/ion collision pairs. The total number of candidate collision partners within a cell is determined using Bird's No-Time-Counter (NTC) method [*Bird*, 1994]. The probability of a collision event is then determined for these candidate pairs based on the total collision cross section.

Analysis by *Boyd and Dressler* [2002] and experimental measurements by *Pullins et al.* [2000] and *Miller et al.* [2002] demonstrate that the $Xe^+ - Xe$ elastic and charge exchange total cross sections are essentially equivalent, such that $\sigma_{MEX} \approx \sigma_{CEX}$. Assuming this is also true for the current study, this allows for the use of a single total cross section (TCS) σ and the relative collision velocity, g, to determine the probability P of a collision event according to

$$P_{MEX} = \frac{\sigma g}{(\sigma g)_{max}}, \tag{3}$$

where a candidate pair is selected for collision if $P_{MEX} > \mathcal{R}_u$, in which $\mathcal{R}_u$ is a uniformly distributed random number. If the collision under consideration involves a neutral/ion pair, the probability of a CEX event is taken as $P = 0.5$ [*Boyd and Dressler*, 2002], such that the total probability of a collision resulting in a charge exchange is

$$P_{CEX} = P_{MEX} \times P. \tag{4}$$

This approach is adopted for the $O^+ - Pr$ and $Pr^+ - Pr$ interactions modeled in this chemical system, although the validity of this assumption should be examined through analysis of the differential cross section (DCS) data which are not available for the energy range of interest.

Postcollision velocities involving neutral/neutral collision pairs are assumed to follow isotropic scattering, while collisions involving neutral/ion pairs scatter anisotropically, with a strong forward scattering tendency. This anisotropic scattering is incorporated into the MPIC CEX model through the use of experimental DCS data. Figure 1 presents measurements of the absolute DCS for CEX scattering of $O^+(^4S)$ with H_2O at 500 eV obtained by *Lindsay et al.* [2001]. These measurements were acquired over a limited range of scattering angles, from 0.04 to 2.9° in the laboratory frame of reference. While many of the scattered particles were found to lie within this narrow range, a comparison of the DCS, integrated from 0 to 3.0°, to an *estimated* TCS indicates that the DCS measurements in Figure 1 capture approximately 74% of the estimated TCS shown in Figure 2. Although the energies considered in this work are significantly lower than those presented in Lindsay *et al.*, this appears to be the only differential cross section data available for the $O^+ - H_2O$ system, for either ground state $O^+(^4S)$ or metastable $O^+(^2D, ^2P)$.

To use this data within the MPIC framework, the differential cross section data is first converted from a laboratory (LAB) frame of reference to the center-of-mass (COM) frame of reference according to *Katz et al.* [2001]:

$$\frac{d\sigma}{d\Omega_{LAB}} = \frac{d\sigma}{d\Omega_{COM}} 4 \cos\theta_{LAB}, \tag{5}$$

where $d\Omega$ is the solid angle and θ is the scattering angle. The resulting distribution is then normalized by the maximum value, and postcollision scattering angles are thereby sampled. To account for the possibility of a large-angle scattering event, the DCS for a $Xe^+ - Xe$ system at 300 eV, plotted in Figure 1, is used for angles larger than 3°. The probability of a postcollision scattering angle larger than 3° is less than 0.025, so inclusion of this data for large scattering angles has a small impact on the postcollision distributions.

As mentioned before, the typical collision energies considered in this work are O(10) eV, which are considerably lower than the energies presented in the total cross section data of Lindsay et al. Fortunately, several measurements of the total cross section for the $O^+(^4S) - H_2O$ system are available at lower energy [e.g., *Turner and Rutherford*, 1968; *Dressler et al.*, 1996; *Li et al.*, 1995]. The total cross section for the $O^+(^4S) - H_2O$ system used in this work is fitted from measurements by Dressler et al. and Lindsay et al. shown in Figure 2. MEX collisions for $Pr - O$, $O - O$, and $Pr - Pr$ are modeled using variable hard sphere

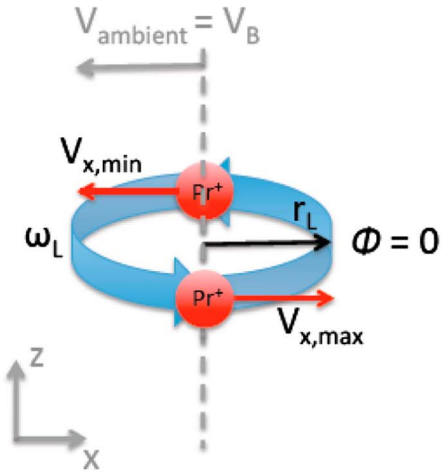

(a) Magnetized Pr^+ ion with gyroscopic motion about magnetic field line.

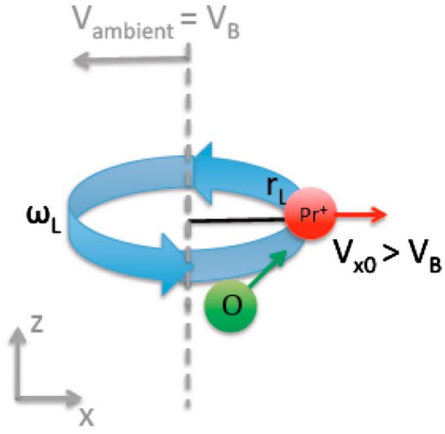

(b) Magnetized Pr^+ ion undergoes MEX collision with either O or Pr. Postcollision velocity of Pr^+ is used to update the phase angle.

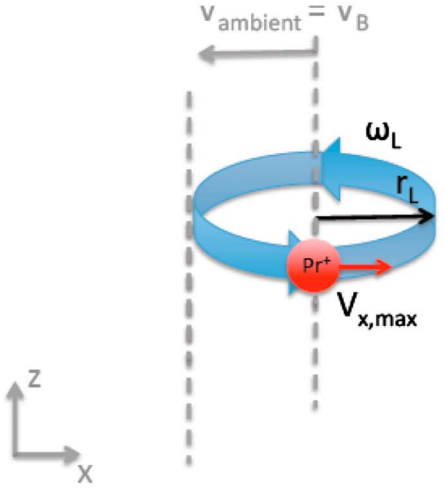

(c) Updated phase angle defines new guiding center, providing a mechanism for cross-field diffusion within the magneticfield model.

Figure 3. Schematic of ion interaction with magnetic field: (a) Magnetized Pr+ ion with gyroscopic motion about magnetic field line. (b) Magnetized Pr+ ion undergoes MEX collision with either O or Pr. Postcollision velocity of Pr+ is used to update the phase angle. (c) Updated phase angle defined new guiding center, providing a mechanism for cross-field diffusion within the magnetic field model.

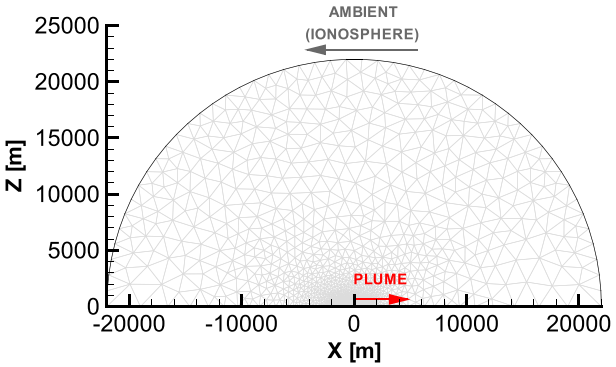

Figure 4. DSMC/PIC computational domain. Axis of symmetry lies along the *x* axis, and the nozzle exit plane is located at the origin. Arrows indicate the plume/ambient flow directions for the ram flow configuration.

(VHS) [*Bird*, 1994] total cross sections and isotropic scattering. The corresponding VHS parameters including the reference diameter d_{ref}, reference temperature T_{ref}, and temperature exponent ω, are provided in Table 2.

2.3. Magnetic Field Model

In addition to CEX interactions, charged particles in LEO are subject to interaction with Earth's magnetic field. The interaction of spacecraft ions with the magnetic field plays an important role in the evolution of the ion plume. Both the strength of the magnetic field and the orientation of the field lines relative to the plume propagation have a substantial impact on the development of the plume, as magnetization of spacecraft ions can impede ion flow in the axial and radial directions. The magnetic field model developed for this work investigates the impact of magnetic field strength on the spacecraft ion plume formation assuming a fixed field line orientation relative to the spacecraft.

Immediately after a CEX event, the newly formed ion enters into a gyroscopic orbit about a magnetic field line. This orbit is characterized by the Larmor radius, r_L, and the gyration frequency, ω_L, which are determined according to

$$r_L = \frac{V_{x0}^{\text{Pr}^+}}{\omega_L}, \tag{6}$$

$$\omega_L = \frac{q^{\text{Pr}^+} B}{m^{\text{Pr}^+}}. \tag{7}$$

In equation (6), $V_{x0}^{\text{Pr}^+}$ is the initial *x* velocity of the Pr^+ species entering the gyroorbit, which is equivalent to the postcollision *x* velocity after a charge exchange reaction. In equation (7), $q^{\text{Pr}+}$ is the fundamental

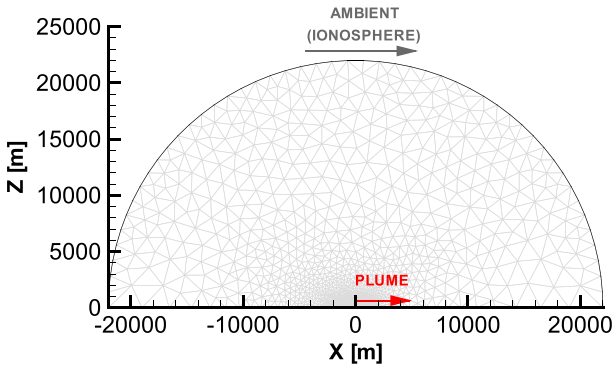

Figure 5. DSMC/PIC computational domain. Axis of symmetry lies along the *x* axis, and the nozzle exit plane is located at the origin. Arrows indicate the plume/ambient flow directions for the wake flow configuration.

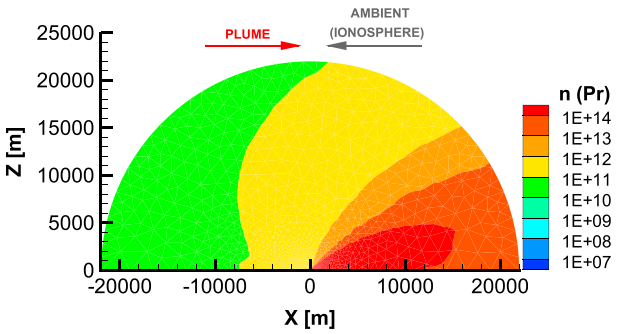

Figure 6. Contours of Pr number density [m^{-3}] formed in the ram flow configuration, assuming $B \rightarrow 0$.

charge, B is the magnetic field strength, and m^{Pr+} is the molecular mass of the Pr^+ species. From these expressions, it is clear that the magnetic field strength uniquely determines the gyration frequency for a given charged chemical species. The Larmor radius, however, is dependent on both magnetic field strength (through ω_L) as well as on the translational energy of the magnetized ion orthogonal to the field line.

Within the present axisymmetric simulations, the magnetic field lines are assumed to be oriented vertically (parallel to the z axis, shown by Figures 3–5, dashed lines). Thus, only the x velocity component of the magnetized ions follows a gyroscopic motion, while the z velocity component is unimpeded by the magnetic field. Magnetized ions entering a gyroscopic orbit with a nonzero velocity component along the field line thus follow a helical trajectory. The frame of reference is held fixed to the spacecraft thruster at the origin, such that the ambient flow, and hence the geomagnetic field lines, has a velocity equivalent to the orbital velocity relative to the spacecraft. The gyroscopic motion due to the magnetic field is imposed on the Pr^+ ions through a time-dependent velocity, which for a constant magnetic field aligned with the z axis, is determined according to

$$V_x^{\text{ion}} = V_B \pm (V_{x0}^{\text{ion}} - V_B) \sin\left(\frac{q^{\text{ion}} B}{m^{\text{ion}}} t + \phi^{\text{ion}}\right), \tag{8}$$

$$\phi^{ion} = \begin{cases} \pi/2 & \text{if } V_{xo}^{\text{ion}} < V_B, \\ 3\pi/2 & \text{if } V_{x0}^{\text{ion}} > V_B. \end{cases} \tag{9}$$

The gyroscopic term on the right-hand side is added when $\phi^{\text{ion}} = 3\pi/2$, and subtracted when $\phi^{\text{ion}} = \pi/2$. The velocity V_{x0}^{ion} is the initial velocity of the magnetized ion as it enters the gyroorbit, which is assumed equal to the postcollision velocity of a Pr^+ ion formed through CEX. When the ion enters the orbit, the phase angle, ϕ^{ion}, is specified according to the relative velocity of the ion with respect to the magnetic field line velocity, V_B. This is shown schematically in Figure 3, for a case in which the ambient flow (and therefore the field line velocity) is directed to the left. If the ion has a velocity to the left relative to the field line, the ion

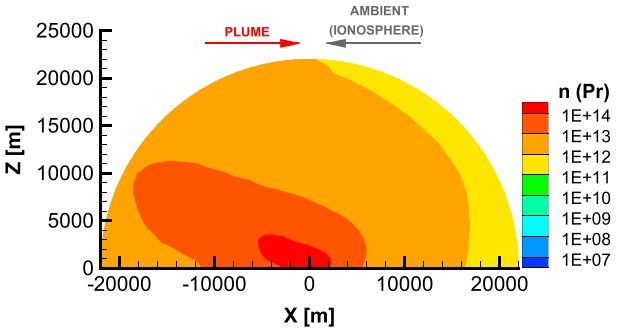

Figure 7. Contours of Pr number density [m^{-3}] formed in the ram flow configuration, assuming $B \rightarrow \infty$.

Table 3. Plume and Ambient Flow Conditions

Species	m (kg kmol^{-1})	k_bT/q_o (eV)	V (m s^{-1})	n (m^{-3})
Pr	20.7	0.06	2990	5.8×10^{23}
Pr^+	20.7	–	–	–
O	16.0	0.06	±7640	9.3×10^{13}
O^+	16.0	0.06	±7640	1.0×10^{11}

enters the orbit with a phase of $\phi^{ion}=\pi/2$. This represents a minimum orbital velocity, and the ion velocity is thus $V_{x0}=V_{x,min}$. If the ion has a velocity to the right relative to the field line, the ion enters the orbit with a phase of $\phi^{ion}=3\pi/2$, and the ion velocity corresponds to $V_{x0}=V_{x,max}$. The time t in equation (8) is initialized to zero when the ion enters the orbit and is advanced by the simulation time step. The gyration frequency in equation (7) is constant and has a value $\omega_L = 233$ rev/s for the $B = 0.5$ Gs cases. The time step used in the simulations is $dt = 2.5\times10^{-4}$ s, and thus, a single gyroscopic orbit is resolved by approximately 17 simulation time steps.

Once magnetized, the motion of the Pr^+ ions is a superposition of the magnetic field velocity and the unsteady gyration velocity in the x direction. In a collisional flow, however, these magnetized ions may undergo collisions with other particles. A collision resulting in both momentum and charge exchange would effectively "demagnetize" the Pr^+ ion, and the resulting Pr neutral would follow a linear trajectory according to its postcollision velocity. This demagnetization process is modeled for Pr^+–Pr charge transfer only, as explained in section 2.2 and summarized in Table 1.

It is also possible for a collision between a magnetized Pr^+ ion and a neutral particle to result in momentum exchange only. Although the Pr^+ ion keeps its charge and remains magnetized, the momentum exchange will effectively bump the Pr^+ onto a new orbit with a new guiding center. This process is shown schematically in Figures 4 and 5, in which a magnetized Pr^+ ion undergoes a MEX collision with an O–atom. In this particular scenario, the Pr^+ ion velocity has a phase $\phi^{ion} = 0$, and thus has zero velocity relative to the field line guiding center. Upon collision, the momentum transfer will result in a finite postcollision x velocity component (e.g., to the right as shown by Figures 4 and 5, red arrow). This postcollision velocity defines the initial velocity V_{x0}^{ion} for a different orbit about a new guiding center, shown in Figure 5. To define the guiding center of the new orbit, the phase angle ϕ^{ion} must be evaluated after each MEX collision using the velocity criteria specified in equation (9), where V_{x0}^{ion} is taken as the Pr^+ postcollision velocity.

This treatment of MEX collisions involving magnetized Pr^+ ions provides a mechanism for cross-field diffusion of the spacecraft ions within these simulations. The cross-field diffusion process is modeled for both Pr^+– Pr and Pr^+– O momentum exchange events, as summarized in Table 1. As mentioned in section 2.2, the ambient O^+ ions are modeled as being trapped indefinitely on the magnetic field lines to preserve the ambient conditions. In consideration of the gyroscopic parameters in equations (6) and (7), the O^+ ions are modeled as magnetized on field lines of infinite strength, $B \to \infty$. The influence of the magnetic field on the spacecraft ions, Pr^+, is examined in this work by considering the limiting cases of $B \to \infty$, $B \to 0$, and the intermediate case of $B = 0.5$ Gs, found in LEO.

2.4. Plume Configurations

The plume flow examined in this study involves the steady firing of a spacecraft thruster into the ambient ionosphere free stream in low Earth orbit. The flow is simulated on an axisymmetric spherical computational

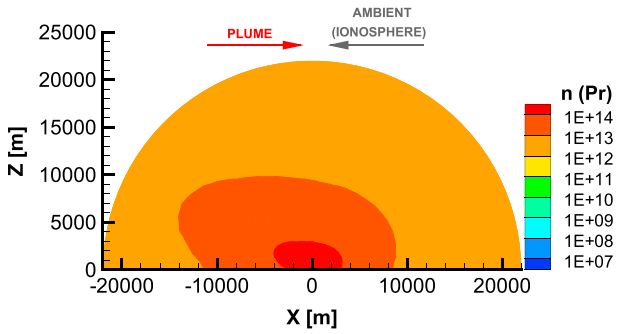

Figure 8. Contours of Pr number density (m^{-3}) formed in the ram flow configuration, assuming $B = 0.5$ Gs. The magnetic field model accounts for the gyroscopic motion of magnetized ions in the LEO case.

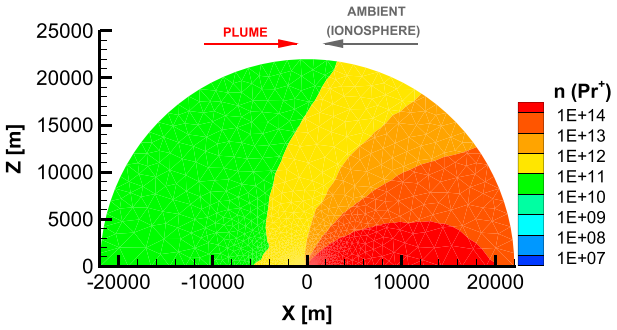

Figure 9. Contours of Pr^+ number density (m^{-3}) formed through charge exchange of the spacecraft neutrals, Pr, with the ambient O^+ ions in the ram flow configuration, assuming $B \rightarrow 0$.

domain shown in Figures 6 and 7, with a radius of 22 km and an axis of symmetry along the x axis. The thruster considered in this study is located at the origin $(x, z) = 0$, and generates thrust in the $-x$ direction, such that the plume flow is initially directed in the $+x$ direction (indicated by Figures 6 and 7, red arrow). An inflow boundary condition is specified at the nozzle exit plane (not visible in Figures 6 and 7), with a nominal mass flow rate typical of the Space Shuttle reaction control system (RCS) jets, $\dot{m} = 4.2$ kg/s. This mass flow rate is based on the known specific impulse and velocity increment for the RCS jets on a fully fueled Orbiter [*Stuit*, 2011] and assuming a simulated nozzle radius of 0.15 m. The plume at the exit plane is modeled as a charge-neutral single species Pr propellant with the properties shown in Table 3. The orbital motion of the spacecraft thruster is equivalent to an ionosphere free stream velocity in either $\pm x$ direction, indicated by Figures 6 and 7 (grey arrow). The ionosphere free stream is comprised of the neutral O−atoms and single charge O^+ ions.

The configuration in which the spacecraft thruster fires against the ambient flow is referred to as the ram flow configuration, shown in Figure 6. The wake flow configuration refers to the case in which the spacecraft thruster fires with the ambient flow, shown in Figure 7. Recalling discussion of the magnetic field model, the magnetic field lines are aligned vertically in these figures, with velocity equal to the ambient velocity. The spacecraft Pr vapor plume expands into the low-density ambient ionosphere and undergoes charge exchange (CEX) collisions, resulting in an ion plume comprised of single-charge Pr^+ ions.

The properties of the plume at the rocket nozzle and the ambient flow are summarized in Table 3. The ambient/inflow properties of temperature, velocity, and number density are specified only for the CEX reactant species initialized as ambient or at the inflow boundary. Constituents of the ambient ionosphere (O, O^+) at an altitude of 400 km are assigned velocities in the $\pm x$ direction, according to the plume configuration being modeled.

3. Results

In this section, steady state results are presented for both the ram and wake flow configurations. In particular, the influence of the magnetic field on the development of both the spacecraft neutral and ion plumes is

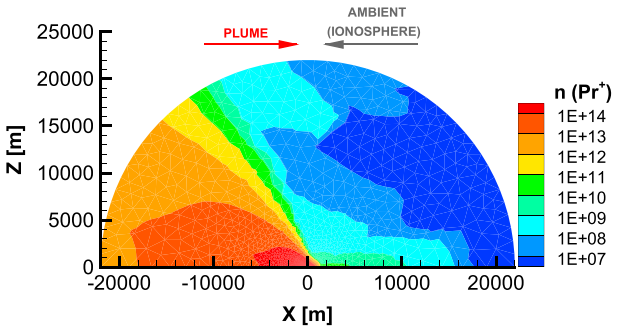

Figure 10. Contours of Pr^+ number density (m^{-3}) formed through charge exchange of the spacecraft neutrals, Pr, with the ambient O^+ ions in the ram flow configuration, assuming $B \rightarrow \infty$.

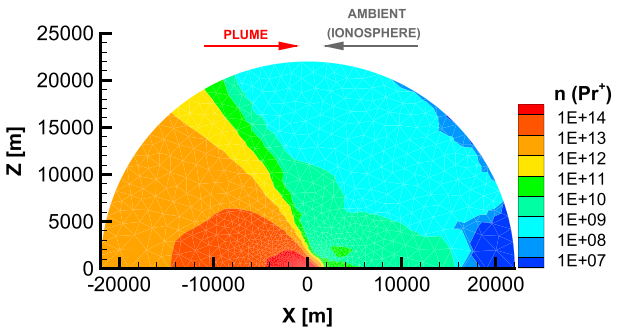

Figure 11. Contours of Pr^+ number density (m^{-3}) formed through charge exchange of the spacecraft neutrals, Pr, with the ambient O^+ ions in the ram flow configuration, assuming $B = 0.5$ Gs.

investigated. Three magnetic field strengths are considered: $B \rightarrow 0$ and $B \rightarrow \infty$ which are the two limiting cases, and an intermediate LEO case in which $B = 0.5$ Gs. Recall that only the Pr^+ ions become magnetized; thus, the magnetic field does not *directly* impact the motion of the neutral Pr particles. It is important to note, however, that the magnetized Pr^+ ions may become demagnetized through CEX reactions, and so the influence of the magnetic field on the development of the neutral Pr plume is examined as well.

All simulation results presented are computed on an unstructured computational mesh with 4600 grid points. The grid points are clustered near the thruster nozzle exit at the origin, where the plume density is highest, and the flow quantities demonstrated convergence in a grid resolution study. These axisymmetric calculations are also sensitive to the number of simulation particles used, particularly in the solution along the axis of symmetry. This is a well-known numerical artifact observed in axisymmetric DSMC simulations. To ensure an accurate solution, the number of particles employed in the numerical simulations are increased until convergence was reached in the plume properties along the axis of symmetry. This required approximately 1.0×10^7 simulation particles in the $B = 0.5$ Gs and $B \rightarrow \infty$ cases, and 2.0×10^7 particles in the $B \rightarrow 0$ cases. Each simulation is run on a cluster of Intel Nehalem processors and required 36 h of compute time on 16 processors.

3.1. Ram Flow Configuration

The steady state flow field generated in the ram configuration is presented in Figures 8–14. The ambient ionosphere flow in this case is from right to left, opposing the plume flow at the origin. In Figures 8–10, the contours represent the number density of the Pr neutrals, which are emitted from the thruster. As the neutral plume expands outward from the thruster, the Pr particles may undergo MEX and CEX collisions with

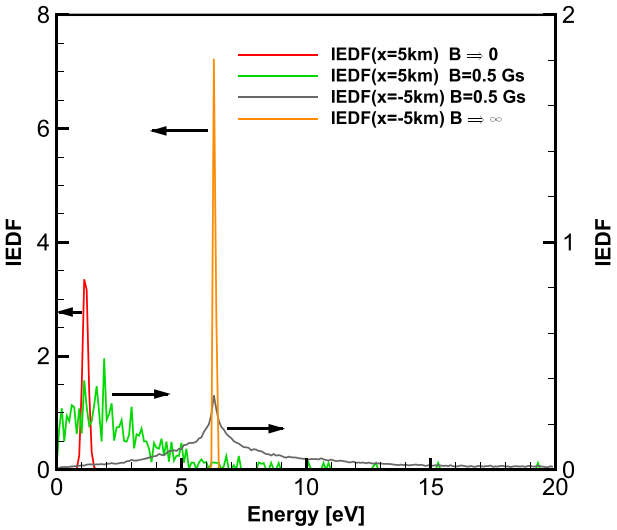

Figure 12. Ion energy distributions sampled ±5 km from the thruster origin. The IEDFs corresponding to $B = 0.5$ Gs account for the gyroscopic motion of magnetized ions.

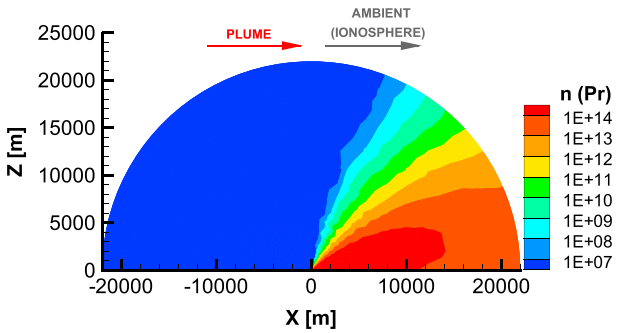

Figure 13. Contours of Pr number density (m^{-3}) formed in the wake flow configuration, assuming $B \rightarrow 0$.

the ambient particles as well as with each other. The first case shows the development of the neutral plume in the absence of a magnetic field, Figure 8. The neutral plume expands outward into the oncoming ambient flow and is largely unaffected by collisions with the relatively low-density ionospheric flow of O and O^+.

Figures 9 and 10 present the development of the spacecraft neutral plume assuming infinite field strength and field strength $B = 0.5$ Gs, respectively. Comparison to Figure 8 shows that the magnetic field has a dramatic effect on the development of the neutral Pr plume. The spacecraft neutral particles are emitted from the thruster in the positive x direction, but in both cases, the neutral plume is pushed downstream of the thruster, in the direction of the ambient flow. Since the magnetic field does not directly modify the motion of the Pr particles, this indicates that the majority of spacecraft neutrals emitted from the thruster undergo CEX to form magnetized Pr^+ ions. These ions are swept downstream by the field lines but then become demagnetized through a subsequent CEX collision. The details by which the ions are magnetized is found to affect the neutral plume shape. The plume in Figure 10 assuming $B = 0.5$ Gs appears more diffuse than the plume under infinite field strength in Figure 9. The neutral plume is found to persist far upstream of the thruster origin under both $B \rightarrow \infty$ and $B = 0.5$ Gs conditions. Under an infinite field strength, the neutral plume propagates 6 km upstream of the thrusters, with a number density of $O(10^{13})m^{-3}$. Considering the magnetic field strength $B = 0.5$ Gs, the neutral plume with number density $O(10^{13})m^{-3}$ is found to propagate 9 km upstream of the thrusters, significantly farther than the infinite field strength model.

This difference in both plume shape and upstream propagation of the neutral plume is largely due to the gyroscopic motion of the magnetized ions that is captured in the $B = 0.5$ Gs model. Recall that ions become demagnetized through a CEX reaction, resulting in the formation of a neutral particle. According to the $B \rightarrow \infty$ model, the precollision velocity of the magnetized ion is equivalent to the orbital velocity, $V_B = -7640$ m/s. The differential cross-section model suggests that CEX interactions for this system are characterized by a strong forward scattering tendency, and so the postcollision velocities of demagnetized Pr particles will generally be in the $-x$ direction. This suggests that most of the Pr neutrals found upstream of the thruster in the $B \rightarrow \infty$ case originate from the thruster and have not yet undergone a CEX collision. Considering the $B = 0.5$ Gs model, ions may become demagnetized at any point on the gyroscopic orbit. This implies that ions may have precollision velocities in either the $+x$ direction or $-x$ direction, depending on

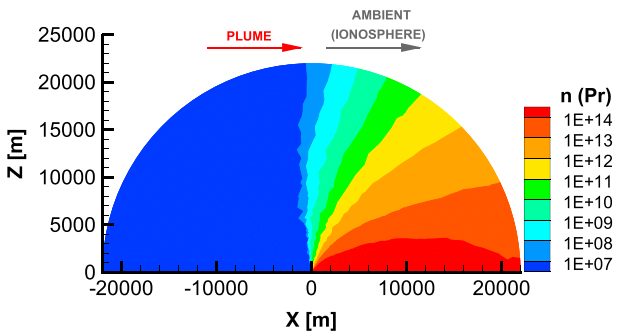

Figure 14. Contours of Pr number density (m^{-3}) formed in the wake flow configuration, assuming $B \rightarrow \infty$.

Table 4. Current Density Due To Cross-Field Diffusion of Pr^+

	Without Cross-Field Diffusion	With Cross-Field Diffusion
+5 km	6.2×10^{-5}(A/m^2)	7.2×10^{-5}(A/m^2) (+16%)
−5 km	7.7×10^{-2}(A/m^2)	9.5×10^{-2}(A/m^2) (+23%)

when the CEX collision takes place. Since the CEX interaction is forward scattering, this results in postcollision Pr velocities in either the $+x$ direction or $-x$ direction, thus enhancing the upstream propagation of the neutral Pr plume.

The steady state flow field generated by the ram configuration is presented again in Figures 11–13 but with focus on the evolution of the ion plume. The contours represent the number density of the Pr^+ ions, which are generated as a result of charge exchange with the ambient O^+ ions. Figure 11 shows the Pr^+ plume development in the absence of a magnetic field. The high-density Pr vapor plume expands outward in the $+x$ direction, at an initial velocity of 2990 m/s. Pr neutrals that undergo CEX with the ambient O^+ have a strong forward scattering tendency. Thus, it is observed that even with the opposing ambient flow, the ion plume propagates in the $+x$ direction. Figure 12 (contours) shows the Pr^+ ion plume in the presence of a magnetic field with infinite strength. In the limit of $B \rightarrow \infty$, the Larmor radius and gyration frequency go to zero and infinity, respectively. Thus, this field strength is modeled by assuming that Pr^+ ions formed through CEX become trapped on field lines immediately, with no gyration. The magnetic field is found to have a significant impact on the plume development, as shown in Figure 12. Pr^+ ions are found upstream of the thruster, but these are ions generated from neutral Pr vapor that convects upstream against the ambient ionosphere flow. Once these neutral particles undergo CEX, they are immediately trapped on the field lines and move in the $-x$ direction with the velocity of the field lines, −7640 m/s. Note that although the magnetic field generally constrains the upstream propagation of the ion plume, the Pr^+ ions are still free to move along the field lines in the $\pm z$ direction.

The intermediate case, $B = 0.5$ Gs, is shown in Figure 13. Pr^+ ions that form through CEX are assumed to gyrate about the field lines with frequency $\omega_L = 233$ rev/s, and a Larmor radius determined by the postcollision velocity immediately after the charge exchange collision. For an ion with a velocity of 2990 m/s and a field line velocity of −7640 m/s, the corresponding Larmor radius is approximately 45 m. The ion plume is qualitatively similar to the $B \rightarrow \infty$ case in Figure 12. The ion plume number density downstream of the thruster is slightly higher in the $B \rightarrow \infty$ case.

The ion energy distribution functions (IEDF) of the Pr^+ ions are compared in Figure 14 for the three field strengths. The distributions are sampled at locations ±5 km from the thruster origin, and 1 km above the axis of symmetry. The IEDF is determined for only those ions which cross the sampling surface in the radial direction outward from the thruster. In the case of infinite field strength, a trace amount of Pr^+ ions are generated upstream at the +5 km sampling location through charge exchange. These ions, however, are immediately magnetized and swept downstream in the $-x$ direction and are thus never counted in the IEDF. The IEDF for the $B = 0.5$ Gs case is reported at both ±5 km sampling locations. Similar to the $B \rightarrow \infty$ case, few ions are found at the 5 km location. However, Pr^+ that are formed upstream become trapped on field lines, and the gyration motion carries these ions across the sampling region.

Several interesting observations may be made from these energy distributions. It is first noted that the IEDF of Pr^+ ions sampled 5 km upstream of the thruster origin is centered over approximately 1 eV. This energy

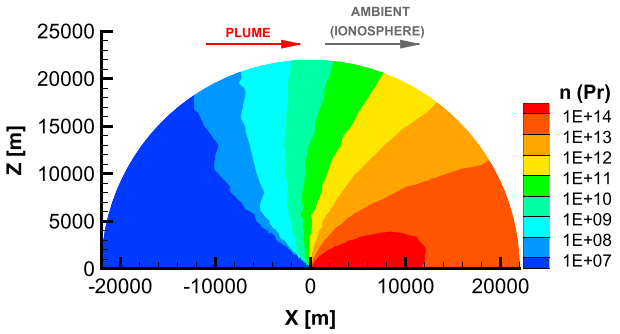

Figure 15. Contours of Pr number density (m^{-3}) formed in the wake flow configuration, assuming $B = 0.5$ Gs, which accounts for the gyroscopic motion of magnetized ions.

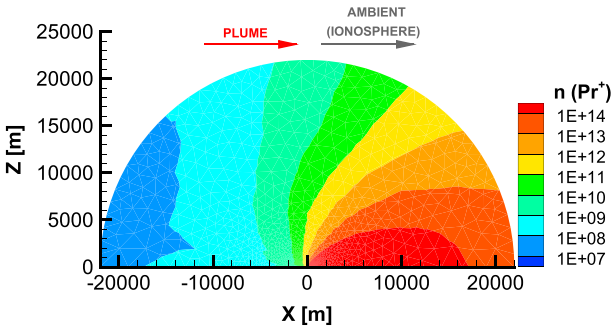

Figure 16. Contours of Pr^+ number density (m^{-3}) formed through charge exchange of the spacecraft neutrals, Pr, with the ambient O^+ ions in the wake flow configuration, assuming $B \rightarrow 0$.

corresponds to the initial energy of the thruster Pr particles. Thus, the Pr neutrals suffer little momentum exchange with the oncoming ambient flow, prior to charge exchange. The differential cross section for the $O^+ - Pr$ system produces a strong forward scattering tendency, thus little momentum is transferred during the charge exchange process. This is observed for both the $B \rightarrow 0$ and $B = 0.5$ Gs cases. However, the IEDF for $B = 0.5$ Gs (shown by Figure 14, green curve), although centered over 1 eV, is very wide in comparison to the peaked IEDF for $B \rightarrow 0$. The effect of the magnetic field is thus to broaden the energy distribution of the magnetized ions, which is consistent with the unsteady gyration motion imposed on the magnetized Pr^+ ions in the x direction. A similar trend is found through comparison of the IEDF sampled at −5 km from the thruster origin. The IEDF of both $B = 0.5$ Gs and infinite field strengths is centered over 6.5 eV, which corresponds to the energy of the Pr^+ with ambient velocity. The IEDF corresponding to the LEO field strength is very broad in comparison to the IEDF of the infinite field strength case.

The influence of the cross-field diffusion is also examined for the $B = 0.5$ Gs case. Recalling from section 2.3, diffusion of the Pr^+ ions across the magnetic field lines is modeled through MEX collisions, in which new guiding centers are determined based on the postcollision velocity and phase angle of the magnetized ion. To disable this cross-field diffusion, the MEX collisions of $O - Pr^+$ and $Pr - Pr^+$ are processed, but the phase angle is not updated. This subsequently increases/decreases the Larmor radius of the magnetized Pr^+ ions, but they remain fixed on the same guiding center until they become demagnetized through a CEX reaction. The ram flow simulation is recomputed using this model, and comparisons of the current density with and without cross-field diffusion are presented in Table 4. The current density is reported at locations ±5 km from the thruster origin. Cross-field diffusion is found to increase the current density, as ion flux is enhanced through this diffusion mechanism.

3.2. Wake Flow Configuration

The steady state flow field generated in the ram configuration is presented in Figures 15–19. The ambient ionosphere flow in this case is from left to right, in the direction of the plume flow at the origin. The contours

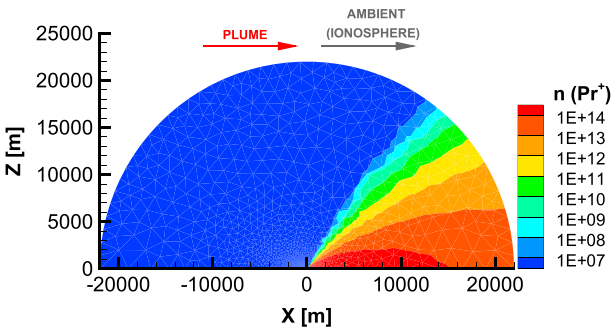

Figure 17. Contours of Pr^+ number density (m^{-3}) formed through charge exchange of the spacecraft neutrals, Pr, with the ambient O^+ ions in the wake flow configuration, assuming $B \rightarrow \infty$.

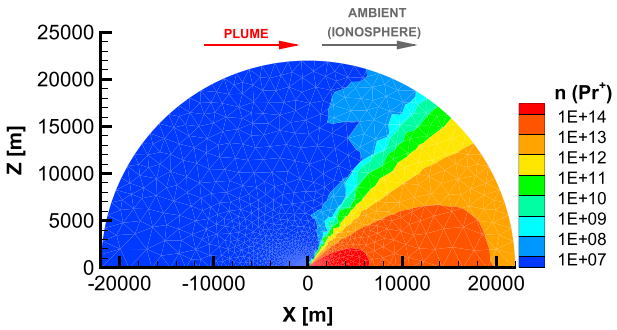

Figure 18. Contours of Pr^+ number density (m^{-3}) formed through charge exchange of the spacecraft neutrals, Pr, with the ambient O^+ ions in the wake flow configuration, assuming $B = 0.5$ Gs.

represent the number density of the neutral spacecraft particles, Pr, which are emitted from the thruster. The first case shows the development of the neutral plume in the absence of a magnetic field, Figure 15. The neutral plume expands outward into the ambient coflow and is again largely unaffected by collisions with the relatively low-density ionospheric flow of O and O^+, even more so than the ram flow configuration shown in Figure 8.

Figures 16 and 17 present the development of the spacecraft neutral plume assuming infinite field strength and field strength $B = 0.5$ Gs, respectively. Comparison to Figure 15 shows that the magnetic field does influence the development of the neutral Pr plume, although the influence is minor compared to the ram flow configuration. The neutral plumes in both cases appear to spread outward and slightly upstream compared to the neutral plume in Figure 15, although the direction of plume propagation in Figures 16 and 17 are generally in the $+x$ direction.

The steady state flow field generated by the wake configuration is again shown in Figures 18–19. Here the contours represent the number density of the ion species, Pr^+. Figure 18 shows the ion plume development in the absence of a magnetic field. The plume development is qualitatively very similar to the $B \rightarrow 0$ results from the ram flow configuration, although the ion density upstream is reduced by approximately 2 orders of magnitude, owing to the wake flow configuration. It is interesting to note that although the neutral Pr particles are restricted mostly downstream of the thruster, the ions are found upstream of the thruster in the absence of the magnetic field. The IEDF for this $B \rightarrow 0$ wake flow configuration is nearly identical to the

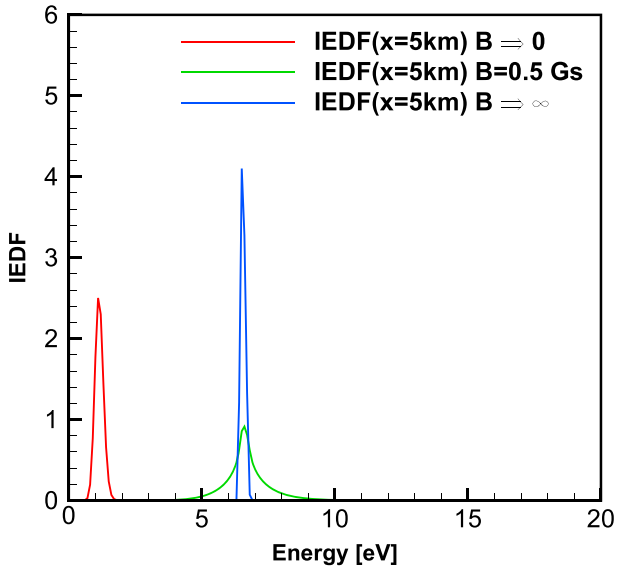

Figure 19. Ion energy distributions sampled ± 5 km from the thruster origin. The IEDFs corresponding to $B = 0.5$ Gs account for the gyroscopic motion of magnetized ions.

$B \rightarrow 0$ ram flow IEDF. It can be concluded then that the flow direction of the ambient ionosphere relative to the spacecraft plume has very little impact on the ion energy distribution when the magnetic field model is not included.

Figure 19 (contours) shows the Pr^+ plume development under a magnetic field of infinite strength. Comparison to the $B \rightarrow \infty$ ram flow configuration in Figure 12 shows a dramatic difference in the ion plume development, as the plume is constrained to the $+x$ direction. The spreading of the ion plume in the $+z$ direction (along the field lines) is less pronounced in this case as well. Recalling that the geomagnetic field lines have the same velocity as the ambient flow, the magnetized ions are swept in the direction of the ambient flow, at the orbital velocity. The IEDF for this case is reported only for the +5 km location, as the IEDF at the −5 km location is not populated. This distribution of Pr^+ ion energy in the wake flow configuration is nearly identical to the $B \rightarrow \infty$ IEDF from the ram flow configuration. This is consistent with the energy of magnetized ions that have a velocity equivalent to the orbital velocity.

The development of the ion plume under a magnetic field strength of $B = 0.5$ Gs in the wake flow configuration is shown in Figure 19. The plume looks qualitatively similar to the plume in Figure 12. The IEDF for $B = 0.5$ Gs is shown in Figure 19, at a location 5 km from the thruster origin. Again, the IEDF is centered over 6 eV, which corresponds to the energy of the magnetized ions that travel with the velocity of the magnetic field lines. The IEDF corresponding to $B = 0.5$ Gs is again broadened as a result of the gyroscopic motion, although this broadening is more substantial in the ram flow configuration. This is consistent with the fact that the ions that become magnetized in the ram flow configuration have a higher velocity relative to the field lines (approximately 10 km/s) compared to the wake flow configuration (approximately 4 km/s).

4. Summary and Conclusions

The primary focus of this work was to examine the development of a steady spacecraft ion plume formed through charge exchange (CEX) reactions with the ambient ionosphere flow in low Earth orbit (LEO). Also of great interest was the influence of the geomagnetic field on the ion plume. To this end, two plume configurations, referred to as ram flow and wake flow, were examined under varying magnetic field strengths. A combined DSMC/PIC methodology was used to properly capture the nonequilibrium collisional and plasma phenomena that are relevant in the rarefied plasma environment in LEO.

The development of the spacecraft neutral and ion plume was first examined in the ram flow configuration, under three magnetic field strengths: two limiting cases, in which $B \rightarrow 0$ and $B \rightarrow \infty$, and $B = 0.5$ Gs, which corresponds to the field strength at LEO. The development of both the neutral Pr plume and the Pr^+ ion plume were strongly influenced by the presence of the magnetic field. The assumption of an infinite field strength provided a reasonable approximation to the more sophisticated model used for $B = 0.5$ Gs. The former assumed magnetized ions have a Larmor radius of zero and are thus trapped on the field lines without a superimposed gyration motion in the x direction. The latter accounted for this finite gyration velocity, and the effect of this gyroscopic motion is to broaden the Pr^+ IEDF. The impact of cross-field diffusion on the current density was also examined for the $B = 0.5$ Gs case and was found to increase the current density due to an enhancement of Pr^+ ion flux across field lines.

Similar results were obtained in the wake flow configuration. The ion plumes generated under the three magnetic field strengths were qualitatively similar, as the ambient flow (and thus magnetic field lines) was in the same direction as the plume flow. The observed Pr^+ IEDFs again demonstrated the broadening of the distribution due to the gyroscopic motion of the magnetized ions.

The assumption of a thruster plume comprised of a single chemical species in this work allowed for a fundamental study of plume/ionosphere interaction in the presence of a geomagnetic field. An improved model should include the major chemical reactants of the hypergolic propellant system, which involves the reaction of both fuel and oxidizer to produce water vapor, among other products. It would therefore be desirable to obtain detailed differential and total cross sections for this mixture of chemical species at the appropriate Low Earth Orbit energies. Although the present simulations are limited to axisymmetric flows, it would be of great interest to extend the present simulations to three-dimensional cases. This would allow for the characterization of plume/ionosphere interactions regardless of the relative orientation of the plume and the geostationary magnetic field lines.

Acknowledgments
We gratefully acknowledge the support of Air Force Research Laboratory (AFRL) Space Vehicles Directorate and Barron Associates, Inc. Work was performed under subcontract to Barron Associates, Inc. through AFRL contract FA9453-11-C-0181. Computational resources and technical support were provided by the Center for Advanced Computing at the University of Michigan.

Robert Lysak thanks Paul Bernhardt and an anonymous reviewer for their assistance in evaluating this paper.

References

Bernhardt, P., et al. (2012), Ground and space-based measurement of rocket engine burns in the ionosphere, *IEEE Trans. Plasma Sci.*, *40*(5), 1267–1286.

Bird, G. (1994), *Molecular Gas Dynamics and the Direct Simulation of Gas Flows*, Oxford Univ. Press, Oxford, U. K.

Birdsall, C., and A. Langdon (2004), *Plasma Physics Via Computer Simulation*, Taylor and Francis, New York.

Boyd, I. (1996), Conservative species weighting scheme for the direct simulation Monte Carlo method, *J. Thermophys. Heat Tr.*, *10*(4), 579–585.

Boyd, I., and R. Dressler (2002), Far field modeling of the plasma plume of a hall thruster, *J. Appl. Phys.*, *92*(4), 1764–1774.

Burke, W., L. Gentile, J. Machuzak, D. Hardy, and D. Hunton (1995), Energy distributions of thruster pickup ions detected by the shuttle potential and return electron experiments during TSS 1, *J. Geophys. Res.*, *100*(A10), 19,773–19,790.

Cai, C. (2005), Theoretical and numerical studies of plume flows in vacuum chambers, PhD dissertation, University of Michigan, Ann Arbor, Mich.

Drakes, J., and D. Swann (1999), DSMC computations of the Progress-M spacecraft retrofiring exhaust plume, *AIAA Paper No. AIAA-99-0975*.

Dressler, R., M. Bastian, D. Levandier, and E. Murad (1996), Empirical model of the state-to-state dynamics in near-resonant hyperthermal $X^{+}+H_2O$ charge-transfer reactions, *Int. J. Mass Spectrom. Ion Processes*, *159*, 245–256.

Kaplan, C., and P. Bernhardt (2010), Effect of an altitude-dependent background atmosphere on shuttle plumes, *J. Spacecraft Rockets*, *47*(4), 700–703.

Karabadzhak, G., Y. Plastinin, B. Khmelinin, V. Teslenko, N. Shvets, J Drakes, D. Swann, and W. McGregor (1997), Experimentation using the Mir station as a space laboratory, *AIAA Paper No. AIAA-97-0288*.

Katz, I., G. Jongeward, V. Davis, M. Mandell, I. Mikellides, R. Dressler, I. Boyd, K. Kannenberg, J. Pollard, and D. King, (2001), A Hall effect thruster plume model including large-angle elastic scattering, *AIAA Paper No. AIAA-2001-3355*.

Li, X., Y.-L. Huang, G. Flesch, and C. Ng (1995), Absolute total cross sections for the ion-molecule reaction $O(^{+})((^{4})S(^{0})) + H(_{2})O$, *J. Chem. Phys.*, *102*(12), 5100–5101.

Lindsay, B., R. Rejoub, D. Sieglaff, and R. Stebbings (2001), Charge transfer of keV $O(^{+})$ ions with CO and H_2O, *J. Phys. B: At. Mol. Opt. Phys.*, *34*, 2159–2165.

McMahon, W., R. Salter, R. Hills, and D. Delorey (1983), Measured electron contribution to shuttle plasma environment, *AIAA Paper No. AIAA-83-2598*.

Miller, S., S. Pullins, D. Levandier, Y. Chiu, and R. Dressler (2002), Xenon charge exchange cross sections for electrostatic thruster models, *J. Appl. Phys.*, *91*(3), 984–991.

Pullins, S., Y. Chiu, D. Levandier, and R. Dressler (2000), Ion dynamics in Hall effect and ion thrusters: $Xe(^{+})$ + Xe symmetric charge transfer, *AIAA Paper No. AIAA-00-0603*.

Stuit, T. (2011), Designing the STS-134 re-rendezvous: A preparation for future crewed rendezvous missions, *AIAA Paper No. 2011-7189*.

Turner, B., and J. Rutherford (1968), Charge transfer and ion-atom interchange reactions of water vapor ions, *J. Geophys. Res.*, *73*, 6751–6758.